Article

Simulation of the Coronal Dynamics of Polymer-Grafted Nanoparticles

Carolyn A. Miller and Michael J. A. Hore*

Read Online

ACCESS | 📊 Metrics & More | 📰 Article Recommendations | 🆂🅸 Supporting Information

ABSTRACT: Polymer-grafted nanoparticles (PGNPs) are an important component of many advanced materials. The interplay between the nanoparticle surface curvature and spatial confinement by neighboring chains produces a complex set of structural and dynamical behaviors in the polymer corona surrounding the nanoparticle. For example, experiments have shown that the inner portion of the corona is more stretched and relaxes more slowly than the outer region. Here, we perform systematic core-modified dissipative particle dynamics (CM-DPD) simulations and analyze the relaxation dynamics using proper orthogonal decomposition (POD) of the monomer coordinates. We find that grafted chains relax more slowly than free chains and that the relaxation time of the grafted chains scales inversely with the confinement strength.

For PGNPs in a polymer melt, the relaxation processes are always Rouse-like. However, we observe either Zimm-like or Rouse-like dynamics for PGNPs in solution depending on the confinement strength.

KEYWORDS: polymer-grafted nanoparticles, polymer dynamics, dissipative particle dynamics
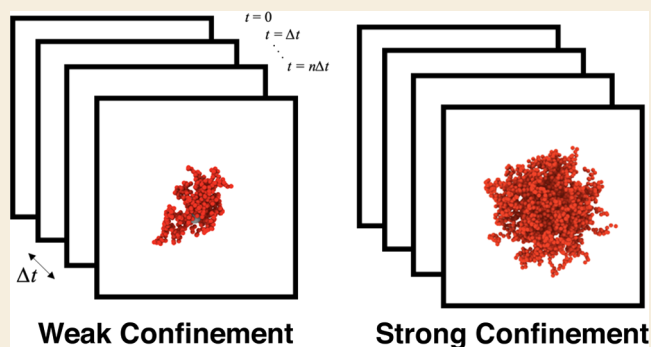
■ INTRODUCTION

The dynamics of polymer chains play an important role in many physical properties of polymeric materials such as the characteristics of the stress relaxation modulus $G(t)$, fracture mechanics, transport phenomena, energy dissipation, and many others.[1−7] When polymers do not entangle, their dynamics can be described in a couple of ways. The Rouse description of the dynamics is based on a friction coefficient for segments of the polymer chain (ζ_p) that scales linearly with the number of monomers in that segment (i.e., $\zeta_p = p\zeta_0$). The resulting diffusion coefficient for the chain produces a spectrum of relaxation times corresponding to relaxations that occur across different length scales or equivalently different groups of monomers. As a result, the relaxation time of each mode p is expressed as

$$\tau_p = \frac{\eta_s b^3}{k_B T}\left(\frac{N}{p}\right)^{1+2\nu} = \tau_0 \left(\frac{N}{p}\right)^{1+2\nu} \tag{1}$$

where η_s is the local viscosity, b is the Kuhn length, ν is the Flory exponent, and N is the degree of polymerization of the chain.[1] The longest relaxation time τ_1, corresponding to that of the entire chain, is referred to as the Rouse time. The Zimm description of polymer dynamics is based on a friction coefficient that is proportional to the size of the chain or segment of interest (i.e., $\zeta_p = \eta_s R$). As a result, it is sensitive to hydrodynamic effects and the relaxation time of each mode

adopts a similar expression to eq 1, but with a scaling exponent of 3ν instead of $1 + 2\nu$. The Zimm model is most appropriate for dilute chains at concentrations much less than the overlap concentration ($\phi \ll \phi^*$), whereas the Rouse model is better suited for unentangled polymer melts. While the success of the Rouse model is typically attributed to a lack of hydrodynamic effects, simulations[8−10] and experiments[8,11] have observed deviations from its predictions of the internal dynamics of polymer chains. These deviations may be due to considerations that are absent from the Rouse model such as interactions.

The above discussion of relaxation times can be formulated in terms of the dynamic structure factor $S(\mathbf{Q}, t)$, which can be helpful in connecting simulations to experimental scattering measurements. Under this description, for length scales less than the size of the polymer, the incoherent dynamic structure factor

$$S_{inc}(\mathbf{Q}, t) \sim \sum_m \exp\left\{-\frac{Q^2}{6}[r_m(t) - r_m(0)]^2\right\} \sim \exp\left(\frac{t}{\tau_Q}\right)^\alpha \tag{2}$$
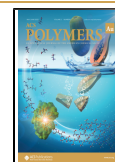
where the value of α depends on the model describing the polymer dynamics. In general, the mean-squared displacement (MSD) of monomer m will evolve according to $\langle \Delta r^2 \rangle = \langle [r_m(t) - r_m(0)]^2 \rangle \sim t^{\alpha}$, where $\alpha = 2\nu/(2\nu + 1)$ in the Rouse model and $\alpha = 2/3$ for the Zimm model.[1] This implies that $\tau \sim R_g^{(2\nu + 1)/\nu}$ for Rouse dynamics and $\tau \sim R_g^3$ for Zimm dynamics, where R_g is the root-mean-squared radius of gyration of the polymer.[12] On the one hand, this means that in dilute solutions, the relaxation times of the polymer scale with the cube of R_g regardless of the conformation of the polymer. On the other hand, this also means that a polymer's excluded volume can influence relaxation times according to the Rouse model. Similarly, others have found that if active forces are present, their influence tends to speed up the dynamics of polymer chains depending on the magnitude and time scale of the active force.[13−15] This enhancement of the dynamics is characterized by an increase in the value of α signifying some degree of directed motion, which, in turn, results in a weaker scaling of the relaxation times with N than would be expected from classical theories alone. Du et al.[15] specifically observed that α increased as the magnitude of the active force increased. If $\alpha = 1$, as in normal diffusive processes, then one predicts $\tau \sim R_g^2$, while $\tau \sim R_g$ for a ballistic process ($\alpha = 2$). Thus, the scaling of τ with R_g weakens as α increases.

In this article, we examine the relaxation dynamics of polymer chains that are grafted to spherical nanoparticle cores using core-modified dissipative particle dynamics (CM-DPD) simulations. Over the past decade or more, a multitude of investigations have sought to understand the behavior of polymers in this coronal layer.[2,3,6,16−26] For example, dynamic light scattering (DLS),[17−19] transmission electron microscopy (TEM),[2,22] and small-angle neutron scattering (SANS)[26−28] have all found that at high values of grafting density (σ), the grafted polymers form a brush that can be subdivided into two regions of concentration. Near the nanoparticle surface, a high density of monomers results in a concentrated polymer brush (CPB). In the CPB, polymer chains are highly stretched due to confinement by neighboring chains and the height of the brush in this region scales as $h \sim N^{4/5}$. As the distance from the nanoparticle core increases, the concentration of polymer decreases, and past a cutoff distance r_c, a semidilute polymer brush (SDPB) forms. In this region, the conformation of the chain relaxes and approaches that of an unconfined polymer (e.g., $h \sim N^{3/5}$ in a good solvent). Although the appearance of two regions of concentrations follows from the predictions of Daoud and Cotton for star polymers,[29] the theory itself does not produce the scaling of h with N. These values have been determined experimentally. Nevertheless, more detailed models[30,31] predict a variety of scaling exponents, depending on the curvature of the underlying surface.

The conformation of the polymers within the corona can strongly influence the mechanical properties of polymer-grafted nanoparticle (PGNP) nanocomposites. For instance, it has been found that the size of the SDPB region strongly influences the fracture mechanics of a polymer nanocomposite.[2] Short or strongly stretched chains cannot effectively entangle with those on neighboring particles, resulting in brittle composites. In contrast, large SDPB regions lead to crazing. Others have observed that the polymer grafting density impacts the storage and loss moduli, $G'(\omega)$ and $G''(\omega)$, respectively.[6,23,32] Broadband dielectric spectroscopy (BDS) measurements of grafted polyisoprene found that the relaxation times of grafted chains were longer than those of free chains and depend on their molecular weight, grafting density,[23] and nanoparticle concen-

tration.[33] As the molecular weight of the polymer increased, however, the relaxation times between the grafted and free chains became very similar to each other. Presumably, the origin of this behavior lies in the description of the corona from the Daoud−Cotton model. Short chains form a corona that is highly stretched and concentrated leading to longer relaxation times. As the chain length increases, the chains become increasingly unconfined far from the nanoparticle surface and the dynamics more closely resemble those of free chains. In terms of the description of these relaxation times (i.e., Rouse or Zimm), neutron spin echo (NSE) measurements of polystyrene-grafted SiO_2 nanoparticles in the melt showed that at short times the dynamics appeared Zimm-like but that the Zimm model could not describe the dynamics at long times since the intermediate scattering function $I(Q,t)$ did not decay to zero.[34] A similar trend was observed in NSE measurements of carbon black,[35] where the lack of decay in $I(Q,t)$ for large t was attributed to the appearance of breathing modes—collective, transverse motions predicted by de Gennes.[36] Mark et al.[37] performed NSE measurements on one-component nanocomposites and determined that the spatial confinement of grafted polymers within a cone defined by their neighbors results in a slowing down of the dynamics and that while the dynamics of the entire chain slow, local segmental dynamics appear identical to a polymer melt. NSE measurements by Wei et al. of poly(methyl acrylate)-grafted SiO_2 nanoparticles in solution took advantage of isotopic labeling to separately measure the dynamics in the inner and outer regions of the corona.[26] In the inner regions, relaxation times were approximately 2−3 times longer than those in the outer regions, a finding that was consistent with previous BDS measurements. However, in solution, the authors found that the Zimm model appeared to describe the dynamics across all time and length scales and that $I(Q,t)$ fully decayed on the time scale of the measurements. Why the dynamics in the CPB region are 2−3 times slower than in the SDPB region, yet appear to follow the Zimm prediction in both regions, remains an outstanding question that we will attempt to resolve in this article.

Computer simulations offer a means to further explore the relaxation dynamics in spherical brushes, such as the corona of PGNPs. Laradji et al.[38] performed a detailed analysis of ungrafted polymer dynamics in dilute and concentrated solutions using DPD simulations. They observed that DPD simulations of dilute solutions reliably reproduce predictions from the Zimm model ($\tau_1 \sim N^{1.77}$), but as the polymer concentration increased, hydrodynamics were not fully screened and the scaling of the relaxation time was between the Rouse and Zimm predictions ($\tau_1 \sim N^{1.86}$). A better agreement with the Rouse prediction could be obtained by increasing the temperature of the system or, equivalently, lowering the Schmidt number. Spenley[39] found $\tau_1 \sim N^{1.98}$ for a pure polymer melt, in excellent agreement with the Rouse prediction. Molecular dynamics (MD) simulations of polymer nanocomposites have used Rouse mode analysis, which will be described later in this article, to examine the relaxation of the free chains as a function of nanoparticle (NP) size, concentration, and interaction characteristics.[4,40−42] Smith et al. demonstrated that attractive interactions between NPs and polymers result in slower dynamics.[40] In athermal nanocomposites with bare NPs, unentangled chains were largely unaffected by the inclusion of NPs except for NPs whose size approached that of a solvent. The largest impact on the dynamics was observed for entangled chains.[41] These results are largely in agreement with investigations into unentangled polymer dynamics under

cylindrical confinement.[42] The standard Rouse mode analysis is not directly applicable to understanding the dynamics of grafted polymers, however, due to different boundary conditions. Hattemer and Arya analyzed the dynamics of grafted chains using sine functions as a basis to decouple the dynamics versus cosine functions that are used for free chains. They found that in their modified analysis two relaxation times appeared in each mode. The authors attributed one of these times to the relaxation of the grafted polymers and the other to rotational relaxations of the chains about the nanoparticle core. Notably, the autocorrelation functions they obtained in this way did not fully decay to zero.[4] Additional key results from their investigations included that bare and grafted NPs essentially had identical effects on the relaxation dynamics of free chains and grafted polymers exhibited longer relaxation times than free chains. Moreover, the relaxation times of grafted polymers increased as the NP size increased. Simulations from Chremos et al.[43] investigated the behavior of bare and polymer-grafted nanoparticles and found that the structure of the corona strongly influences the diffusivity of the nanoparticle. Finally, Neha et al. demonstrated that PGNPs could be modeled as star polymers with a large, spherical core using a theoretical framework—although they did not explicitly examine the relaxation times of the grafted chains.[44]

Motivated by previous experimental and simulation results, we report in this article an analysis of the relaxation dynamics of grafted polymers from CM-DPD simulations. PGNPs are modeled as star polymers with a large impenetrable core, and the relaxation times of the grafted chains are extracted using proper orthogonal decomposition (POD) to obtain the normal coordinates of the monomers. As we demonstrate below, an advantage to this approach is that it does not require *a priori* knowledge of the necessary basis functions to decouple the dynamics (e.g., cosine functions for standard "Rouse mode analysis"). The relaxation dynamics of the grafted chains are examined in solution and in an unentangled melt for four different confinement strengths and are compared to linear and star polymers with identical chain lengths. The grafted chains had an increased radius of gyration (R_g) relative to free chains, which increased as the degree of confinement increased. We find that relaxation times of the grafted polymers increase as their confinement increases, with dynamics that can be explained by considering the value of α, which describes monomer motions.

■ MODEL AND METHODS

Dissipative Particle Dynamics

The temporal evolution of polymer solutions and melts was simulated using dissipative particle dynamics (DPD) using a parallel, in-house code (PD²). Under this approach, DPD particles correspond to fluid/polymer elements that may contain many "physical" atoms. The DPD particles interact via a conservative force, which accounts for interactions between particles, as well as a random and dissipative force, which together form the DPD thermostat for the system. These pairwise forces are expressed as

$$\mathbf{F}_{ij}^C = a_{ij} w^R(r_{ij}) \hat{\mathbf{r}}_{ij} \tag{3}$$

$$\mathbf{F}_{ij}^D = -\gamma w^D(r_{ij})(\hat{\mathbf{r}}_{ij} \cdot \mathbf{v}_{ij}) \hat{\mathbf{r}}_{ij} \tag{4}$$

and

$$\mathbf{F}_{ij}^R = \frac{\sigma}{\sqrt{\Delta t}} w^R(r_{ij}) \theta_{ij} \hat{\mathbf{r}}_{ij} \tag{5}$$

with $\mathbf{r}_{ij} = \mathbf{r}_i - \mathbf{r}_j$, $\mathbf{v}_{ij} = \mathbf{v}_i - \mathbf{v}_j$, $r_{ij} = |\mathbf{r}_{ij}|$, and $\hat{\mathbf{r}}_{ij} = \mathbf{r}_{ij}/r_{ij}$. θ_{ij} is a symmetric random variable with zero mean and unit variance, uncorrelated for different times and particle pairs. The strength of the conservative force is governed by the coefficient a_{ij}, and the force is weighted by a factor that sets the length scale of the simulation (r_c)

$$w^R(r_{ij}) = w(r_{ij}) = \begin{cases} (1 - r_{ij}/r_c), & r_{ij} < r_c \\ 0, & r_{ij} \geq r_c \end{cases} \tag{6}$$

r_c was set equal to 1. Although not required, a common choice for the dissipative weighting factor is $w^D(r_{ij}) = w^2(r_{ij})$, which is used here. To maintain thermal equilibrium, the fluctuation−dissipation theorem requires that the coefficients of the dissipative and random forces be related as $\sigma^2 = 2\gamma k_B T$. The friction parameter $\sigma = 3.0$. In DPD units, $k_B T = \epsilon_0 = 1.0$. To reproduce good solvent conditions, the strength of the conservative interaction between polymer (P) and solvent (S) is set such that $a_{PS} = a_{PP} = a_{SS} = 25\epsilon_0/r_c$. In a polymer melt, as will be shown below, these interaction parameters result in neutral interactions and ideal chain characteristics. As noted previously, DPD preserves hydrodynamics[38,45] and these interaction parameters provide a good solvent condition in solution.[38,39] Simulations were performed at a fixed density of $\rho = 3r_c^{-3}$.

Neighboring beads in each polymer chain were connected using a FENE potential

$$U_F(r_{i,i+1}) = \begin{cases} -\dfrac{k_F}{2}(r_{max} - r_{eq})^2 & r_{i,i+1} < r_{max} \\ \ln\left[1 - \left(\dfrac{r_{i,i+1} - r_{eq}}{r_{max} - r_{eq}}\right)^2\right], & \\ \infty, & r_{i,i+1} \geq r_{max} \end{cases} \tag{7}$$

with $k_F = 40\epsilon_0/r_c^2$, $r_{max} = 2r_c$, and $r_{eq} = 0.7r_c$. Finally, the positions and velocities for a given particle i are governed by the equations

$$\frac{d\mathbf{r}_i}{dt} = \mathbf{v}_i \tag{8}$$

and

$$\frac{d\mathbf{v}_i}{dt} = \frac{1}{m_i} \mathbf{F}_i \tag{9}$$

where m_i is the mass of bead i, and $\mathbf{F}_i$ is the net force acting on that particle. For simplicity, $m_i = 1$ for all monomers and solvent particles. Although entanglements can be modeled in DPD by including a segmental repulsive potential,[46,47] we opted to omit it for simplicity and restricted our focus to short, unentangled chains. Equations 8 and 9 are solved using the velocity-Verlet algorithm, with $\Delta t = 0.001\tau_0$ as the integration time step.

Initially, PGNPs were placed at random locations in the system and all polymers were initialized with a random configuration and random velocity. Systems were equilibrated until the temperature converged to $k_B T = 1.0$ and the root-mean-squared radius of gyration converged to a constant value. R_g fluctuated by no more than $0.001r_c$ over the duration of the simulation. The equilibration process was accomplished after approximately 50 000 time steps for $N \leq 30$ and approximately 100 000 time steps for $N \geq 50$. After equilibration, the structure and dynamics of the polymers were observed over 1−30 million production steps, depending on the degree of polymerization of the grafted chains, until the normal mode autocorrelation function $C_p(t)$, described below, decayed below 0.1. R_g and the longest relaxation time, τ_1, were obtained from a single trajectory for each set of parameters. However, we performed multiple simulations on select systems to ensure that our values of R_g and τ_1 were reproducible and representative of the true values.

Core-Modified DPD

Polymer-grafted nanoparticles were modeled using core-modified DPD (CM-DPD). CM-DPD, introduced by Whittle and Travis,[48] is an
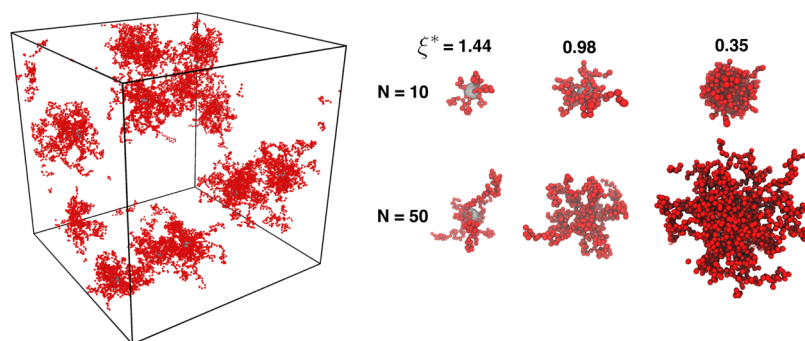
Figure 1. (Left) Representative snapshot of a typical simulated system. For clarity, the solvent has been omitted. The volume fraction of PGNPs shown is $\phi_{NP} = 0.1$. (Right) Representative snapshots of nanoparticles grafted with polymers with chain lengths of $N = 10$ and $N = 50$. ξ^* is a confinement parameter (described below) that decreases as the polymer grafting density increases.
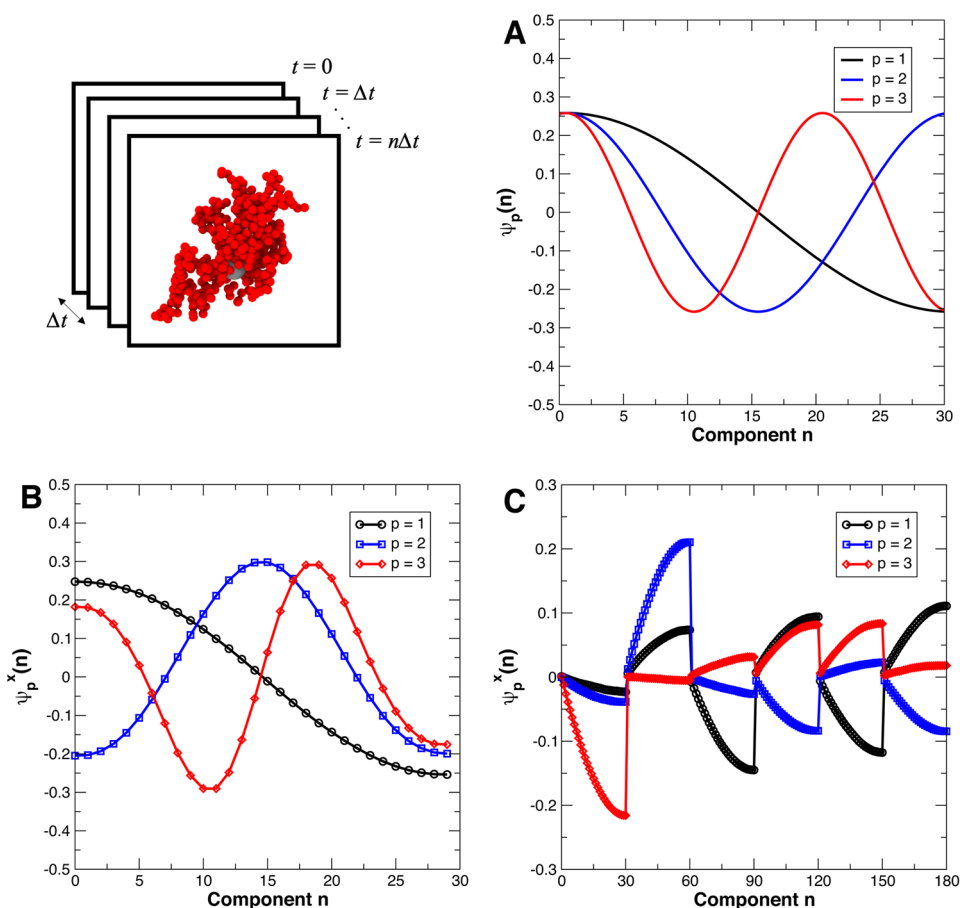
Figure 2. Proper orthogonal decomposition (POD) computes the relaxation modes from snapshots of the monomer positions, as depicted in the illustration. Comparison between (a) the basis functions from the Rouse model for the first three modes ($p = 1-3$) for a linear polymer with $N = 30$ and (b) the first three eigenvectors from POD for the same polymer. Note that $p = 1$ is the eigenvector with the largest eigenvalue, $p = 2$ is that with the second largest eigenvalue, and so on. (c) First three eigenvectors obtained from POD for an $f = 6$-arm star polymer with $N_{arm} = 30$ and a total degree of polymerization of $N = 1 + fN_{arm} = 181$.

extension to the standard DPD framework, which allows calculations using beads with a finite size, rather than the point-like particles used in traditional DPD. This extension has enabled facile simulations of colloids and does not require the use of rigid-body dynamics to integrate the equations of motion. For two interacting particles i and j, the weighting factor is modified to read

$$w^R(h_{ij}) = w(h_{ij}) = \begin{cases} (1 - h_{ij}/r_c), & h_{ij} < r_c \\ 0, & h_{ij} \geq r_c \end{cases} \quad (10)$$

where the surface-to-surface separation distance $h_{ij} = r_{ij} - R_i - R_j$. For all simulations, $R_i = 0$ if the particle belongs to the solvent or a polymer chain and $R_i = R_{NP}$ if the particle represents the nanoparticle core. The size of the grafted monomers was fixed at $R_{mon} = 0r_c$ (i.e., the standard DPD implementation). Penetration of the interior of the nanoparticle by solvent and/or polymer beads was mitigated by including a repulsive force $F_{ij}^{core} = f_{core} = 500\epsilon_0\hat{r}_{ij}$ if $h_{ij} < 0$. To model PGNPs, the objects are represented as star polymers with an impenetrable core of radius $R_{NP} = 1.15r_c$. This value was chosen to most effectively map the simulations onto previous NSE studies by Wei et al.[26] For pure star polymer simulations, $R_{NP} = 0$ to relax the impenetrability of the core bead. The

polymer arms are attached to the core through a FENE potential, with $r_{max} = (2 + R_{NP})r_c$ and $r_{eq} = (0.7 + R_{NP})r_c$ to reflect the larger size of the core bead.

The larger core-modified beads have a corresponding increased mass. Whittle and Travis suggested that if the density of the core-modified bead is set equal to that of the surrounding fluids, then its mass should be rescaled as $m_i = (2R_i + 1)^3$.[48] We verified that the mass of the central NP core does not influence the value and scaling relationships of R_g and τ_p. A typical system and representative nanoparticles for select values of the polymer chain length N and confinement parameter ξ^* (described below) are shown in Figure 1. Because the number of PGNPs in the systems were kept fixed, the volume fraction of the polymer is not fixed in the system. The system shown in Figure 1 is at a volume fraction of $\phi_{NP} = 0.1$—the largest value we considered.

Proper Orthogonal Decomposition

Proper orthogonal decomposition (POD) was performed to extract the normal coordinates for the polymer chains, from which the relaxation dynamics can be analyzed. In standard simulations of linear polymers,[40−42] these normal coordinates are the Rouse coordinates

$$\mathbf{X}_p(t) = \sqrt{\frac{2}{N}} \sum_{i=1}^{N} \cos\left[\frac{p\pi}{N}\left(i - \frac{1}{2}\right)\right]\mathbf{r}_i(t) \tag{11}$$

which are cosine transforms of the monomer positions at time t, $\mathbf{r}_i(t)$.[49] However, as noted by others,[4,50,51] for grafted polymers and nonideal conformations, these coordinates may not represent the true normal coordinates, which can complicate the analysis of polymer dynamics. To overcome this, Wong and Choi[52] showed that the normal modes can be obtained numerically through POD. Under this approach, a covariance matrix with elements C_{ij} is constructed from the time-averaged fluctuations in the positions of monomers i and j from the center of mass of the polymer as

$$C_{ij}^q = \frac{1}{T} \sum_{t=0}^{T-1} q_i'(t)q_j'(t) \tag{12}$$

where q is the x, y, or z component of $\mathbf{r}(t)$. T is the total number of snapshots from the trajectory of the system, and the fluctuations in the positions each monomer from the center of mass of the chain are given by

$$q_i'(t) = q_i(t) - \frac{1}{N} \sum_{j=1}^{N} q_j(t) \tag{13}$$

The three spatial components were treated separately in our analysis, and the results are averaged to reduce statistical deviations. Note that eq 12 implies that the matrix is self-adjoint and that the eigenvalues are guaranteed to be real. The normalized eigenvectors of this matrix, $\tilde{\psi}_p^q$, when ordered by the *decreasing* value of their corresponding eigenvalue describe relaxations at progressively shorter times/smaller length scales. The comparison between the classical result from Rouse and eigenvectors obtained from POD is shown in Figure 2a,b, demonstrating that the two approaches produce similar results and that the eigenvector with index p represents relaxations of the pth Rouse mode for linear chains. However, as will be discussed later, this correspondence is not true for star polymers/PGNPs. For comparison, the first three eigenvectors for an $f = 6$-arm star polymer, with each arm having a degree of polymerization $N_{arm} = 30$ ($N = 1 + fN_{arm} = 181$), are shown in Figure 2c. The eigenvectors consist of f segments of length N_{arm}, separated by $(f − 1)$ nodes, where $\psi_p^x(kN_{arm}) = 0$. The normal coordinates of the polymer are then given by the transformation

$$\mathbf{X}_p^q(t) = \sum_{n=1}^{N} \tilde{\psi}_p^q(n)q_n(t) \tag{14}$$

where $\tilde{\psi}_p(n)$, with $n \in [1, N]$, is the nth component of the eigenvector, and $q_n(t)$ is the coordinate of monomer n in the chain. $\tilde{\psi}_p^q(n)$ is analogous to the cosine term in eq 11.

The characteristic relaxation times described by each eigenvector p can be extracted by computing the normalized time autocorrelation for the normal coordinates obtained from that eigenvector. This was computed separately for each chain in the system and averaged across the ensemble of all chains. The autocorrelation function is expected to decay as

$$C_p(t) = \frac{\langle \mathbf{X}_p(t) \cdot \mathbf{X}_p(0) \rangle}{\langle \mathbf{X}_p(0) \cdot \mathbf{X}_p(0) \rangle} \approx \exp\left[-\left(\frac{t}{\tau_p}\right)^{\beta_p}\right] \tag{15}$$

with $\beta_p \approx 1$. Wong and Choi[52] noted that in their POD analysis of molecular dynamics simulations β_p tended to fall between 0.95 and 1.05. If β_p was treated as a free parameter in our fits of $C_p(t)$, we found it to be converged to $0.9 \leq \beta_p \leq 1.1$. For the results presented in the following sections, we set $\beta_p = 1$, which resulted in a good fit ($R^2 \geq 0.95$).

■ RESULTS AND DISCUSSION

Linear and Star Polymers

To verify that POD produces a correct description of polymer dynamics in DPD simulations, we first considered linear and star homopolymers with chain lengths between $N = 10$ and $N = 100$ in the melt and dilute solution states. The logarithm of the root-mean-squared radius of gyration (R_g) is plotted as a function of the logarithm of the number of segments in the chain in Figure 3a, along with linear least-squares fits (solid lines). The results confirm that in the melt, linear chains have a size that scales as $R_g \sim N^\nu$ in the melt, with $\nu = 0.51$. In solution, we found that $\nu = 0.58$. Both values of the Flory exponent agree with predictions from classical theories[1] as well as DPD simulations by others.[38,39]

In Figure 3b, the normalized time autocorrelation function $C_p(t)$ of the normal coordinates is plotted for linear chains in the melt (circles) and solution (squares) for the longest mode ($p = 1$). The functions all decay exponentially with $\beta_p = 1$ and are equivalent to those obtained using Rouse mode analysis (not shown), implying that POD correctly produces the expected relaxation characteristics. In addition, the similarity means that the $p = 1, 2, 3, ..., N$ eigenvectors from POD can be directly mapped onto the $p = 1, 2, 3, ..., N$ Rouse modes for linear chains. The relaxation times of the chains were extracted by fitting $C_p(t)$ to eq 15 and are plotted in Figure 3c on a double-logarithmic scale. The solid lines are linear least-squares fits to obtain the scaling exponents. In the melt, the longest relaxation time $\tau_1 \sim N^{1.97}$, where the scaling exponent is close to the prediction from the Rouse model of $1 + 2\nu = 2.02$ and in quantitative agreement with previous results from Spenley.[39] In solution, where the hydrodynamic effects are assumed to accelerate relaxation times, we find $\tau_1 \sim N^{1.81}$, which is in accord with the Zimm model prediction of $3\nu \approx 1.76$ and in exact agreement with previous results from Laradji et al.[38] Thus, the combination of DPD simulations and POD correctly reproduces the expected scaling of the chain size and relaxation times for linear polymers and exactly matches the results of previous DPD simulations using Rouse mode analysis.

Because we model PGNPs as star polymers with a large, impenetrable spherical core, we next investigated the scaling relationships between R_g, τ_p, and N that are produced from DPD simulations of simple star polymers with $f = 6$ arms. These polymers have a central bead with a size that is identical to the monomer size. We considered the case of star polymers in the melt, solution, and in a melt of linear chains with a degree of polymerization equal to the degree of polymerization of a single arm of the star, N_{arm}. R_g for a single arm is plotted as a function of $(N_{arm} − 1)$ on a double-logarithmic scale for these three systems
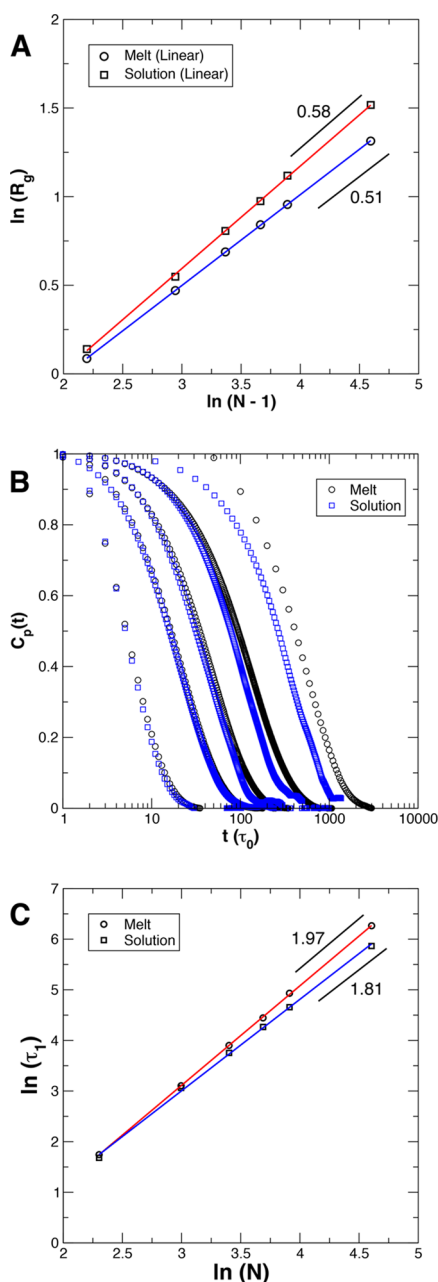
Figure 3. (a) Scaling relationship for the root-mean-squared radius of gyration (R_g) of linear chains as a function of the number of bonds in the chain. The numerical values correspond to the value of the Flory exponent ν determined from least-squares fitting. (b) Normal coordinate autocorrelation functions obtained from POD for linear polymers in solution (blue squares) and in the melt (black circles). From left to right, sets of curves correspond to N = 10, 20, 30, 50, and 100. (c) Scaling relationship of the longest relaxation time, extracted from panel (b), of the chain with N. The scaling exponent of τ_1 is indicated near each curve.

in Figure 4a. While the star polymers in a pure melt and a melt of linear chains exhibit ν = 0.51, we find a weaker scaling of R_g in solution (ν = 0.52) compared to linear polymers. Nevertheless, the solution results are in quantitative agreement with our previous experimental SANS measurements of poly(N-isopropyl acrylamide) star polymers in D_2O with 3 $\leq f \leq$ 6.[53] Although we cannot definitively identify the source of this weaker scaling, we speculate that a higher concentration of monomers near the core of the molecule may lead to a weaker

scaling relationship due to the expulsion of solvent in the interior of the star and a corresponding partial screening of excluded volume interactions.[54]

Zimm and Kilb[55] investigated the relaxation dynamics of branched polymers analytically by deriving the normal modes of symmetric and asymmetric star polymers. Their results indicated that if the eigenvectors, which decouple the dynamics of star polymers, contain nodes, even-numbered modes will vanish and the eigenvectors/eigenvalues for odd-numbered modes will occur as degenerate sets with a multiplicity of ($f-1$) for each mode. Thus, the first three eigenvectors shown in Figure 2c all describe the same relaxation process in the star polymer and correspond to the longest mode p = 1. In addition, Zimm and Kilb demonstrated that the relaxation time of each mode is equivalent to that of a linear polymer that has an effective degree of polymerization $N_{eff} = 2(fN_{arm} + 1)\ /f$. The modes in this case represent relaxations of two arms connected to the central core bead. The autocorrelation function $C_p(t)$ for a star polymer with N_{arm} = 100 and f = 6 is plotted in Figure 4b for $p = 1-11$ (p odd). As predicted by Zimm and Kilb, groups of ($f - 1$) autocorrelation functions appear, all with similar relaxation times. By plotting τ_p as a function of (N_{eff}/p) (Figure S1, Supporting Information), we confirmed that only odd-numbered modes appear on the basis of their position on a master curve, and we indexed the actual mode numbers as denoted in the annotations in the figure. In Figure 4c, we compare the autocorrelation functions for p = 1 for star polymers with (left to right) N_{arm} = 10, 20, 30, 50, and 100 in both a melt of linear chains with $N = N_{arm}$ and in a dilute solution. Unlike in the case of linear chairs, $C_p(t)$ looks very similar for all values of N in both the melt and solution states—indicating similar values and scaling of τ_1 with N.

The Zimm and Rouse times for a polymer chain scale with N to a power that depends on the Flory exponent, which is different for our star polymers than for linear polymer chains. To eliminate the dependency on ν, the longest relaxation time can be plotted as a function of R_g, where $\tau_1 \sim R_g^3$ for the Zimm model and $\tau_1 \sim R_g^4$ for the Rouse model, assuming ν = 0.5.[38] In Figure 4d, the relaxation times for linear polymers are plotted as a function of R_g on a double-logarithmic scale, showing that $\tau_1 \sim R_g^{3.0}$ in solution and $\tau_1 \sim R_g^{3.7}$ in the melt (black dashed lines), both of which are in agreement with theory. Also shown in the figure are the relaxation times for the star polymers (blue points) in the melt (filled diamonds), solution (triangles), and linear melt states (open diamonds), where the lines are least-squares fits to determine the scaling exponents. τ_1 is increased for the star polymers relative to the linear polymers because each relaxation time corresponds to that of a linear chain with $N_{eff} = 2(fN_{arm} + 1)\ /f$, as described above. However, the scaling of τ_1 with R_g is different for star polymers than for linear polymers due to effects that are not captured by a different value of N. Whereas linear chains in solution exactly follow the predictions of Zimm, star polymers in solution exhibit relaxation times that scale as $\tau_1 \sim R_g^{3.3}$ ($\tau_1 \sim N^{1.81}$), which deviates from the Zimm prediction of $\tau_1 \sim R_g^3$ and is likely Rouse-like. Earlier experiments from Richter et al. observed signs of hydrodynamic screening in star polymer solutions.[54] In a melt of identical star polymers, $\tau_1 \sim R_g^{3.5}$, which is a weaker scaling than both the Rouse prediction and our simulations of linear chains. When fit as a function of N, we find that melts of star polymers display relaxation times that scale as $\tau_1 \sim N^{1.86}$, which is intermediate between the Rouse and Zimm predictions. Finally, when star polymers are dispersed in a melt of identical linear chains, $\tau_1 \sim R_g^{3.4}$ ($\tau_1 \sim N^{1.80}$), which is similarly
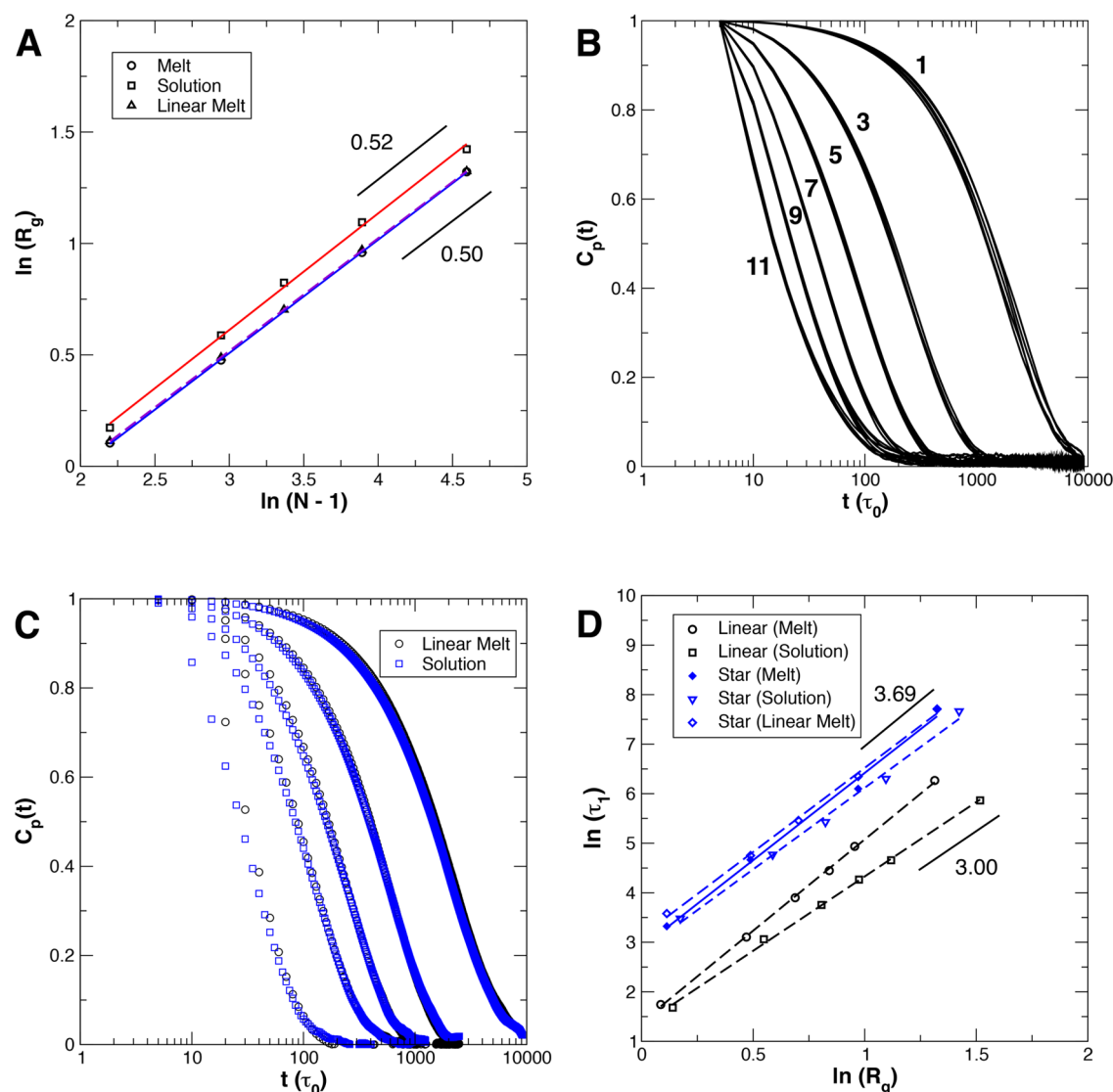
Figure 4. (a) Scaling relationship of R_g for a single arm of $f = 6$-arm star polymers in a melt of identical star polymers (circles), in a dilute solution (squares), and in a melt of identical linear chains (triangles) with $N = N_{arm}$. (b) $C_p(t)$ for a star polymer with $N_{arm} = 100$, showing the $(f-1)$-fold degeneracy of the modes for (right to left) $p = 1, 3, 5, 7, 9,$ and 11. (c) Comparison of $C_p(t)$ between star polymers in a linear melt and solution ($p = 1$) and (d) scaling relationship between the longest relaxation time τ_1 and the root-mean-squared radius of gyration of a single arm. For comparison, the data from Figure 3c for linear chains are shown in black. Lines are least-squares fits to the points.

weaker than one would expect from considering the Rouse model. In summary, star polymer simulations indicate that the relaxation of the arms of the star polymers is Rouse-like but show weaker scaling of τ_1 with R_g and N than predicted from the Rouse model.

If instead the dynamics are examined on the basis of eq 2, the relaxation times of the star polymers imply that $\langle \Delta r^2 \rangle = \langle [r_m(t) - r_m(0)]^2 \rangle \sim t^{0.6}$, which is below the Zimm prediction of $\langle \Delta r^2 \rangle \sim t^{2/3}$ but accelerated relative to the Rouse prediction. This behavior was previously observed in both molecular dynamics and Monte Carlo simulations of linear homopolymers under cylindrical confinement.[56] Brochard and de Gennes calculated that a polymer under cylindrical confinement would show relaxation times that scale as $\tau \sim N^2 D^{1/3}$, where D is the diameter of the cylinder. However, molecular dynamics and Monte Carlo calculations found a weaker scaling of $\tau_1 \sim N^{1.75}$ or equivalently $\tau_1 \sim R_g^{3.5}$, which is in quantitative agreement with the star polymer melt and consistent with our results, which find a weaker-than-expected scaling of τ with R_g in the solution and

linear melt systems. If $\tau_1 \sim N^{1.75}$, then $\langle \Delta r^2 \rangle \sim t^{0.57}$, which is faster than the Rouse model predicts. However, we note that the nature of confinement and the value of D are ill-defined in our simulations of star polymers. Nevertheless, in our simulations, the scaling exponent of $\langle \Delta r^2 \rangle$ is always higher for grafted polymers relative to free chains and is higher in the presence of solvent than in a polymer melt—a behavior that persists in the PGNP systems described in the following sections.

PGNPs in Solution and Linear Melts

To map our CM-DPD simulations to previous experiments,[26] we define a confinement parameter in the same way as the correlation length in the Alexander-de Gennes brush,[1] $\xi^* = 1/\sqrt{\sigma^*}$. The rescaled grafting density $\sigma^* = \sigma R_{g0}^2$, where R_{g0} is the radius of gyration of a free chain with the same degree of polymerization. We calculate σ^* using the radius of the impenetrable core, $R_{NP} = 1.15 r_c$. The confinement parameter represents the average spacing of chains on the nanoparticle surface. Under this definition, if $\xi^* < 1$, the grafted chains are

closer to each other than R_g, and chains begin to be confined by their neighbors. Conversely, $\xi^* \geq 1$ roughly corresponds to an unconfined chain.

We simulated dilute systems with $\xi^* = 2.04$, 1.77, 1.44, 1.12, 0.98, 0.75, 0.46, and 0.35, corresponding to $N_c = 3$, 4, 6, 10, 13, 22, 60, and 100 grafted polymers, respectively. The volume fraction of the PGNPs, which includes both the NP core and grafted polymers, was kept below $\phi_{NP} = 0.1$. Earlier neutron spin echo (NSE) measurements investigated SiO$_2$ nanoparticles ($R_{NP} \approx 10$ nm) that were grafted with poly(methyl acrylate) ($\sigma = 0.3$ chains/nm^2) with a molecular weight of $M_n \approx 30$ kg/mol ($R_g \approx 5$ nm). Therefore, to map our CM-DPD simulations to previous experiments, the closest comparison occurs for $\sigma^* = 7.5$ and $\xi^* \approx 0.35$. The nanoparticle radius was fixed at a value of R_g for linear chains with $N = 10$: $R_{NP} = 1.15\ r_c$. In the rescaled units used in our CM-DPD simulations, the Daoud−Cotton model predicts that the brush should be stretched at distances smaller than

$$r^* = \frac{R_{NP}}{\xi^* \sqrt{N^* \left(\frac{1}{2} - \chi\right)}} \tag{16}$$

where $N^* = 10$ is a reference chain length, and $\chi = 0$ for our choice of parameters. If $r^* < R_{NP}$, then no stretched region is expected in the corona. Equation 16 predicts no stretched region for $\xi^* \geq 1$. For $\xi^* < 1$, eq 16 predicts $r^* = 1.61 r_c$ for $\xi^* = 0.46$ and $r^* = 2.1 r_c$ for $\xi^* = 0.35$.

R_g is plotted as a function of the number of bonds in the chain for the PGNPs in Figure 5. In both solution and a linear melt, R_g adopts a similar value for $\xi^* \geq 1$ and increases more strongly as ξ^* decreases below unity, signifying an increasing amount of confinement. In solution, the grafted chains adopt swollen configurations that are reflective of good solvent conditions ($\nu = 0.6$). Similarly, in a melt of linear chains, the grafted chains adopt an ideal conformation ($\nu = 0.5$). These scaling relationships persist even as ξ^* decreases and confinement increases. We hypothesize that similar scaling exponents reflect the fact that standard DPD beads do not have a well-defined size and can overlap with one another, as depicted in the illustration in Figure 5. For this reason, confinement effects on the chain conformations are diminished. In addition, $2R_g \approx 2.2 r_c$ for $N = 10$, which is larger than the thickness of the predicted stretched region: $h = (r^* - R_{NP}) = 0.46 r_c$ for $\xi^* = 0.46$ and $h = 0.95 r_c$ for $\xi^* = 0.35$. These relatively small values of h compared to $2R_g$ imply that the region of strong confinement is smaller than the size of the polymer chain and contributes only slightly to the scaling of R_g with N. However, in comparison to the star polymer results above which found $R_g \sim N^{0.52}$ in solution, the polymers grafted to the nanoparticles show stronger stretching in solution.

Although the standard DPD implementation of the grafted monomers does not appear to reproduce the large Flory exponent that is observed experimentally, as ξ^* decreases, the grafted polymers are stretched relative to their equilibrium size. In Figure 6a, R_g for each value of N is normalized by the root-mean-squared radius of gyration of a free chain (R_{g0}) and plotted as a function of ξ^*. On one hand, for $\xi^* > 1$, R_g/R_{g0} is not substantially larger than unity but does increase slightly as ξ^* decreases, indicating that the size of the grafted chain is essentially the same as in the ungrafted case and at most $\sim 5\%$ larger. On the other hand, for $\xi^* < 1$, R_g/R_{g0} grows significantly as ξ^* decreases, showing that the close proximity of neighboring chains leads to an increase in the grafted chain size by as much as 25 % due to the increased spatial confinement. Finally, the
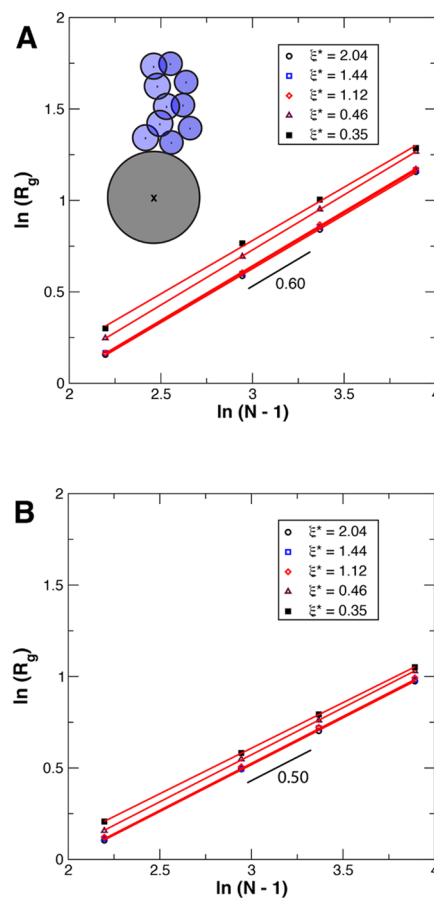

Figure 5. Scaling relationship for the root-mean-squared radius of gyration (R_g) of grafted chains as a function of the number of bonds in the chain in the (a) solution and (b) linear melt states. ξ^* is the confinement variable, which decreases as the chains become more confined. Red lines are least-squares fits, with the slope denoted below.

amount of stretching in the grafted polymers is larger for PGNPs in solution (open squares) than for PGNPs in the melt state (filled circles).

To answer how spatial confinement affects the longest relaxation time τ_1 for the grafted polymers, we plot τ_1 as a function of ξ^* in Figure 6b. Sets of autocorrelation functions for each value of ξ^* are given in the Supporting Information (Figures S2−S17). From bottom to top, sets of points correspond to $N = 10$, 20, 30, and 50. Square points correspond to PGNP solutions, and circles correspond to PGNP melts. We observe that the scaling of τ_1 with ξ^* is similar for each value of N and indeed between the solution (dashed lines) and melt states (solid lines). We define the parameter β to be the magnitude of the slope of each line and find that $\tau_1 \sim (\xi^*)^{-\beta}$. On average, $\beta = 1.28 \pm 0.22$ in solution and $\beta = 1.07 \pm 0.09$ in the melt, where the uncertainty is calculated as the standard deviation of the average. Thus, the value of τ_1 scales approximately with the inverse of ξ^*. The larger value of β in solution is likely the result of the larger Flory exponent for the PGNPs ($\nu = 0.6$), resulting in stronger spatial confinement as ξ^* decreases (i.e., grafting density increases).

Finally, we considered how τ_1 scales with R_g for the grafted chains and extracted the value α that corresponds to the scaling of the mean-squared displacement of a monomer in the chain with time, as discussed above. The results are plotted in Figure 7 and show that in the melt (circles) $\alpha \approx 0.65$ for large values of ξ^*,
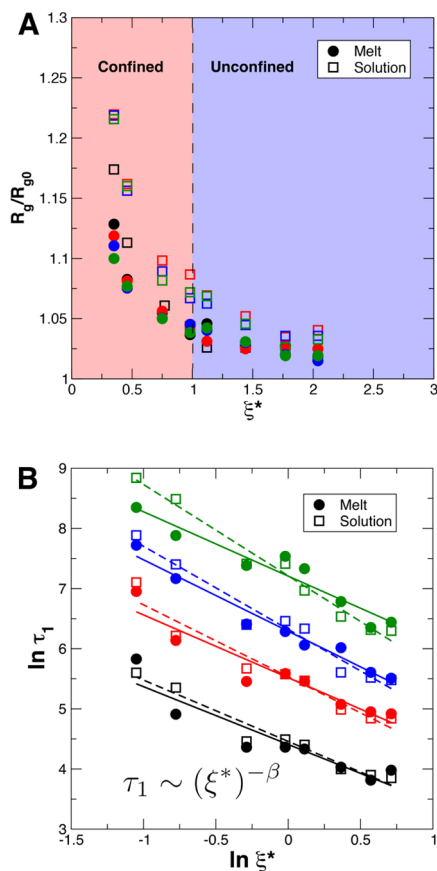
Figure 6. (a) R_g normalized by the radius of gyration of an equivalent free chain (R_{g0}) plotted as a function of the confinement parameter ξ^*. Circles correspond to PGNPs in the melt, and squares correspond to PGNPs in solution. For $\xi^* < 1$, the grafted chains are more strongly confined and show an increase in R_g. (b) Longest relaxation time τ_1 plotted as a function of ξ^*. Solid and dashed lines are least-squares fits to the melt and solution data, respectively, and show that $\tau_1 \sim (\xi^*)^{-\beta}$, with $\beta = 1.07 \pm 0.09$ in the melt and $\beta = 1.28 \pm 0.22$ in solution. The colors of the points correspond to $N = 10$ (black), $N = 20$ (red), $N = 30$ (blue), and $N = 50$ (green).
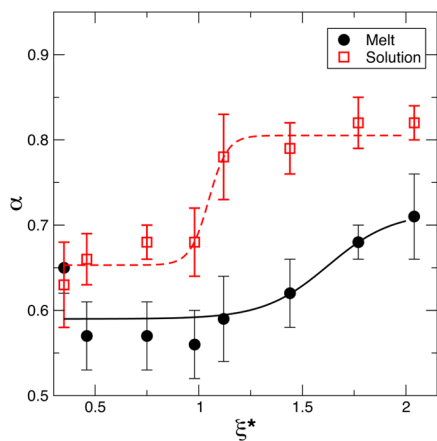
Figure 7. Diffusion exponent α plotted as a function of confinement parameter ξ^*. Circles correspond to PGNPs in the melt and squares correspond to PGNPs in solution. The lines are to guide the eye. In the melt state, $\alpha \approx 0.6$ for all values of the confinement parameter, while in solution, $\alpha \approx 0.8$ for $\xi^* > 1$. Under strong confinement, α is the same between the melt and confinement, implying that the scaling of τ_1 with R_g is similar.

which decreases very slightly to $\alpha = 0.6$ as ξ^* decreases. This may indicate that the diffusion of the monomers is more directed than would be expected on the basis of the Rouse model, which predicts $\alpha = 1/2$. Similarly, the value of α for the PGNPs in solution is higher than either the Zimm or Rouse model would predict. In solution, $\alpha \approx 0.8$ for large values of ξ^* but crosses over to a value of $\alpha \approx 0.65$ for $\xi^* < 1$. This implies that in solution, one would expect approximate scalings of $\tau_1 \sim R_g^{2.5}$ for $\alpha \approx 0.8$ and $\tau_1 \sim R_g^{3.3}$ for $\alpha \approx 0.6$. The higher values of the solutions relative to the melts could be explained, in part, on the basis of the excluded volume, which tends to increase the Flory exponent ν as interactions between the polymer and the environment become more favorable or as the chains become more stretched. For this reason, since ν is larger in the solution systems, one would expect a slightly increased value of α.

The values of α that we obtain from CM-DPD simulations can be understood on the basis of previous quasielastic neutron scattering (QENS) measurements. Neutron backscattering measurements by Jhalaria et al.[3] probed the self-motions of grafted polymers on particles similar to those in our previous NSE measurements and found that the scaling of τ with q transitions from Rouse behavior ($\tau \sim q^{-4} \sim R_g^4$) to diffusive behavior ($\tau \sim q^{-2} \sim R_g^2$) as q increases. This signifies that self-motions are diffusive at small length scales and transition to subdiffusive motions (i.e., Rouse-like motions) at larger length scales in the chain or, equivalently, that α decreases from $\alpha \approx 1$ to $\alpha \approx 0.5$ as q decreases. Thus, the origin of higher values of α that we observe relative to the Rouse prediction may be due, in part, to a crossover from diffusive to subdiffusive motion at the length scales relevant to our CM-DPD simulations. However, a crossover from diffusive to subdiffusive dynamics would be expected to produce a value of α that is always greater than the theoretical prediction (i.e., $\alpha = 1/2$ for Rouse dynamics or $\alpha = 2/3$ for Zimm dynamics). Therefore, our data suggest that for PGNPs in the melt, the relaxation processes are always Rouse-like since $1/2 < \alpha < 2/3$. In contrast, we hypothesize that in solution, for $\xi^* > 1$, the relaxation processes could be Zimm-like since $\alpha > 2/3$, but for $\xi^* < 1$, the relaxation processes must be Rouse-like since $\alpha < 2/3$. This conclusion warrants additional experiments and simulations in the future. Nevertheless, the values we obtain from CM-DPD simulations are consistent with experiments that measure the local dynamics, as we will describe in the following section.

Comparison to Previous Experiments

Several experimental studies in the literature can be used to interpret the results of our CM-DPD simulations.[3,26,32,33,37,57] First, neutron scattering measurements by Mark et al.[37] found that the conformation of grafted chains was not significantly different from free chains. The CM-DPD simulations find similarities and differences to this work. While our simulations show that the Flory exponent of the grafted chains remains identical to free chains, we find that grafted chains can be stretched by as much as 20 % under high confinement ($\xi^* < 1$). The fact that the chains can be stretched agrees well with the work from Bockstaller et al.,[2,22] Hore et al.,[27] Kumar et al.,[18,58] and Ohno et al.[19] However, all of these studies were performed with different techniques and/or analyzed with differing scattering models and not all explicitly evaluated the local conformation.

In terms of dynamics, Mark et al. measured that the dynamics of grafted polymers were slowed relative to free chains at length scales comparable to the entire chain, but that local segmental

dynamics were not affected. These findings agree with BDS measurements from Archer et al.,[23,33] NSE measurements from Wei et al.,[26] and certain features of neutron backscattering measurements from Jhalaria et al.[3] Our CM-DPD simulations find that the longest relaxation time increases as ξ^* decreases as a result of increasing spatial confinement. However, our simulations cannot address whether the local dynamics of the chains are affected by ξ^* because we cannot observe higher modes than $p = 1$ for the PGNP simulations. In addition, because we focused on the case where there are no preferential interactions between the polymers and solvent/matrix, we cannot comment on effects such as interchain interactions.[8−10] However, experiments have demonstrated that attractive polymer−particle interactions can slow polymer dynamics in nanocomposites and in other cases also leave local segmental dynamics unchanged.[57,59,60] In addition, our CM-DPD simulations do not take into account entanglements that may also be an important consideration.[37]

Because we chose parameters that are close to those used in experiments by Wei et al.,[26] we can make more quantitative comparisons to that work. Wei et al. made neutron spin echo measurements[26] at $\xi^* = 0.35$ and observed that the relaxation times of grafted poly(methyl acrylate) scaled with the scattering vector as $\tau \sim q^{-2.5} \sim R_g^{2.5}$ and that the relaxation times in the inner region of the corona were approximately 2−3 times slower than in the outer regions. The results of our CM-DPD simulations find that for the outer region of the corona, $\tau_1 \sim q^{-2.5}$, as was found experimentally. However, we predict a stronger scaling of τ_1 with q than was measured experimentally for the inner region of the corona. Although we cannot say definitively, the origin of this discrepancy could be due to a combination of the length scales that we are probing in NSE and DPD, experimental resolution, a larger value of ξ^* for the inner region of the corona in the experiments than we estimated, the effect of a nonzero value of the Flory−Huggins parameter χ between the polymer and solvent in the experiments, or the fact that experimental measurements probed only a portion of the entire polymer chain while our CM-DPD simulations produce a relaxation time for the entire chain. Regardless, the values of α that we observe are in reasonable agreement with those seen by Wei et al.[26] and Jhalaria et al.[3] and are likely the result of a transition between diffusive and subdiffusive motions.

A final validation of the CM-DPD simulations is to estimate what the difference in τ_1 for the inner and outer regions of the corona would be, assuming that they can be treated independently as they were in experiments. A key result from our simulations is the relaxation time $\tau_1 \sim (\xi^*)^{-\beta}$, with $\beta = 1.28 \pm 0.22$ in solution and $\beta = 1.07 \pm 0.09$ in the melt. From this, we can estimate that the ratio between the relaxation times in the inner (τ_i) and outer regions (τ_o) is related to the ratio of their confinement parameters

$$\frac{\tau_i}{\tau_o} = \left(\frac{\xi_i^*}{\xi_o^*}\right)^{-\beta} = \left[\xi_i^* \sqrt{N^*}\left(\frac{1}{2} - \chi\right)\right]^{-\beta} \tag{17}$$

Note that this equation breaks down in the event that no CPB region exists (i.e., $r^* < R_{NP}$). Using $\xi_i^* = 0.35$, $N^* = 10$, $\beta = 1.28$, and $\chi = 0$, we predict that $\tau_i \approx 2\tau_o$. Thus, our current CM-DPD simulations are in excellent agreement with the measurements from Wei et al.[26] and support the conclusion that the different relaxation rates observed in the inner and outer regions are due primarily to different degrees of confinement. However, on the basis of the CM-DPD simulations and the scaling of τ with q

found experimentally, it may be the case that Zimm dynamics do not govern the relaxation processes in the inner region of the corona as was previously concluded,[26] although additional experiments may be needed to fully address this point.

CONCLUSIONS

In summary, we have performed systematic CM-DPD simulations of PGNPs in the melt and solution states to determine how the structure and dynamics in the corona respond to increasing confinement by neighboring chains. Because the standard Rouse mode analysis is not directly applicable to the case of PGNPs, we used proper orthogonal decomposition (POD) to examine the relaxation dynamics of the grafted chains.

We characterized our PGNPs by a single parameter ξ^*, which describes the degree to which grafted chains are confined, with $\xi^* < 1$ being strongly confined. We find that the ill-defined size of the grafted DPD beads results in the weak scaling of R_g with N compared to what has been generally observed experimentally. However, the grafted chains express larger values of R_g than free chains due to spatial confinement by neighboring chains. A key result from our study is that the longest relaxation time of a grafted polymer scales as $\tau_1 \sim (\xi^*)^{-\beta}$, with β slightly larger than 1 and larger in solution than in the melt. The scaling of τ_1 with R_g is weaker than the classical Rouse predictions, which we attribute to a crossover from diffusive motion at small length scales to subdiffusive motion at larger length scales. Our simulations suggest that for $\xi^* < 1$, the relaxation processes are Rouse-like regardless of whether the PGNPs are in solution or a polymer melt. For $\xi^* > 1$, the relaxation processes are Rouse-like in the melt and may be Zimm-like in solution. Previous QENS measurements[3,26,37] support the results of our simulations.

Looking at the future, additional NSE measurements of PGNPs in both the melt and solution states would be useful to compare to our CM-DPD simulations, which predict that the stretching of the grafted chains should be weaker in the melt and the scaling of τ with q should be stronger than was measured for PGNPs in solution. Additional simulations and theory that can provide more insight into the origin of the elevated values of α that we observe in CM-DPD simulations would provide a clearer molecular-level description of what exactly governs the relaxation of grafted polymers. Such a description is bound to lead to an enhanced understanding of the complex behaviors of PGNPs as we continue to utilize them as components in functional materials for a variety of applications.

ASSOCIATED CONTENT

Supporting Information

The Supporting Information is available free of charge at https://pubs.acs.org/doi/10.1021/acspolymersau.1c00031.

Identification of odd modes of star polymers (Figure S1); autocorrelation functions for PGNP systems (Figures S2−S17); and summary of DPD results (Tables S1−S7) (PDF)

AUTHOR INFORMATION

Corresponding Author

Michael J. A. Hore − *Department of Macromolecular Science and Engineering, Case Western Reserve University, Cleveland, Ohio 44106, United States;* orcid.org/0000-0003-2571-2111; Phone: +1 (216) 368-0793; Email: hore@case.edu

Author

Carolyn A. Miller − *Department of Macromolecular Science and Engineering, Case Western Reserve University, Cleveland, Ohio 44106, United States*

Complete contact information is available at:
https://pubs.acs.org/10.1021/acspolymersau.1c00031

■ REFERENCES

(1) Rubinstein, M.; Colby, R. H. *Polymer Physics*; Oxford university press New York, 2003; Vol. 23.

(2) Choi, J.; Dong, H.; Matyjaszewski, K.; Bockstaller, M. R. Flexible particle array structures by controlling polymer graft architecture. *J. Am. Chem. Soc.* **2010**, *132*, 12537−12539.

(3) Jhalaria, M.; Buenning, E.; Huang, Y.; Tyagi, M.; Zorn, R.; Zamponi, M.; García-Sakai, V.; Jestin, J.; Benicewicz, B. C.; Kumar, S. K. Accelerated Local Dynamics in Matrix-Free Polymer Grafted Nanoparticles. *Phys. Rev. Lett.* **2019**, *123*, No. 158003.

(4) Hattemer, G. D.; Arya, G. Viscoelastic properties of polymer-grafted nanoparticle composites from molecular dynamics simulations. *Macromolecules* **2015**, *48*, 1240−1255.

(5) Hyon, J.; Gonzales, M.; Streit, J. K.; Fried, O.; Lawal, O.; Jiao, Y.; Drummy, L. F.; Thomas, E. L.; Vaia, R. A. Projectile Impact Shock-Induced Deformation of One-Component Polymer Nanocomposite Thin Films. *ACS Nano* **2021**, *15*, 2439−2446.

(6) Hore, M. J. A. Polymers on nanoparticles: structure & dynamics. *Soft Matter* **2019**, *15*, 1120−1134.

(7) Bailey, E. J.; Winey, K. I. Dynamics of polymer segments, polymer chains, and nanoparticles in polymer nanocomposite melts: a review. *Prog. Polym. Sci.* **2020**, *105*, 101242.

(8) Paul, W.; Smith, G. D.; Yoon, D. Y.; Farago, B.; Rathgeber, S.; Zirkel, A.; Willner, L.; Richter, D. Chain Motion in an Unentangled Polyethylene Melt: A Critical Test of the Rouse Model by Molecular Dynamics Simulations and Neutron Spin Echo Spectroscopy. *Phys. Rev. Lett.* **1998**, *80*, 2346−2349.

(9) Paul, W.; Smith, G. D.; Yoon, D. Y. Static and Dynamic Properties of a n-C100H202 Melt from Molecular Dynamics Simulations. *Macromolecules* **1997**, *30*, 7772−7780.

(10) Jeong, C.; Douglas, J. F. Mass dependence of the activation enthalpy and entropy of unentangled linear alkane chains. *J. Chem. Phys.* **2015**, *143*, No. 144905.

(11) Antonietti, M.; Pakula, T.; Bremser, W. Rheology of small spherical polystyrene microgels: a direct proof for a new transport mechanism in bulk polymers besides reptation. *Macromolecules* **1995**, *28*, 4227−4233.

(12) Muthukumar, M. Screening of hydrodynamics in a solution of crumpled manifolds. *J. Chem. Phys.* **1988**, *88*, 2854−2855.

(13) Osmanović, D.; Rabin, Y. Dynamics of active Rouse chains. *Soft Matter* **2017**, *13*, 963−968.

(14) Winkler, R. G.; Elgeti, J.; Gompper, G. Active Polymers - Emergent Conformational and Dynamical Properties: A Brief Review. *J. Phys. Soc. Jpn.* **2017**, *86*, No. 101014.

(15) Du, Y.; Jiang, H.; Hou, Z. Study of active Brownian particle diffusion in polymer solutions. *Soft Matter* **2019**, *15*, 2020−2031.

(16) Kumar, S. K.; Jouault, N.; Benicewicz, B.; Neely, T. Nanocomposites with Polymer Grafted Nanoparticles. *Macromolecules* **2013**, *46*, 3199−3214.

(17) Savin, D. A.; Pyun, J.; Patterson, G. D.; Kowalewski, T.; Matyjaszewski, K. Synthesis and characterization of silica-graft-polystyrene hybrid nanoparticles: Effect of constraint on the glass-transition temperature of spherical polymer brushes. *J. Polym. Sci. Part B: Polym. Phys.* **2002**, *40*, 2667−2676.

(18) Dukes, D.; Li, Y.; Lewis, S.; Benicewicz, B.; Schadler, L.; Kumar, S. K. Conformational Transitions of Spherical Polymer Brushes: Synthesis, Characterization, and Theory. *Macromolecules* **2010**, *43*, 1564−1570.

(19) Ohno, K.; Morinaga, T.; Takeno, S.; Tsujii, Y.; Fukuda, T. Suspensions of Silica Particles Grafted with Concentrated Polymer Brush: Effects of Graft Chain Length on Brush Layer Thickness and Colloidal Crystallization. *Macromolecules* **2007**, *40*, 9143−9150.

(20) Dodd, P. M.; Jayaraman, A. Monte carlo simulations of polydisperse polymers grafted on spherical surfaces. *J. Polym. Sci. Part B: Polym. Phys.* **2012**, *50*, 694−705.

(21) Jayaraman, A.; Schweizer, K. S. Effect of the Number and Placement of Polymer Tethers on the Structure of Concentrated Solutions and Melts of Hybrid Nanoparticles. *Langmuir* **2008**, *24*, 11119−11130.

(22) Choi, J.; Hui, C. M.; Pietrasik, J.; Dong, H.; Matyjaszewski, K.; Bockstaller, M. R. Toughening fragile matter: mechanical properties of particle solids assembled from polymer-grafted hybrid particles synthesized by ATRP. *Soft Matter* **2012**, *8*, 4072−4082.

(23) Kim, S. A.; Mangal, R.; Archer, L. A. Relaxation Dynamics of Nanoparticle-Tethered Polymer Chains. *Macromolecules* **2015**, *48*, 6280−6293.

(24) Koerner, H.; Opsitnick, E.; Grabowski, C. A.; Drummy, L. F.; Hsiao, M.-S.; Che, J.; Pike, M.; Person, V.; Bockstaller, M. R.; Meth, J. S.; Vaia, R. A. Physical aging and glass transition of hairy nanoparticle assemblies. *J. Polym. Sci., Part B: Polym. Phys.* **2016**, *54*, 319−330.

(25) Lee, P. W.; Isarov, S. A.; Wallat, J. D.; Molugu, S. K.; Shukla, S.; Sun, J. E. P.; Zhang, J.; Zheng, Y.; Lucius Dougherty, M.; Konkolewicz, D.; Stewart, P. L.; Steinmetz, N. F.; Hore, M. J. A.; Pokorski, J. K. Polymer Structure and Conformation Alter the Antigenicity of Virus-like Particle−Polymer Conjugates. *J. Am. Chem. Soc.* **2017**, *139*, 3312−3315.

(26) Wei, Y.; Xu, Y.; Faraone, A.; Hore, M. J. A. Local structure and relaxation dynamics in the brush of polymer-grafted silica nanoparticles. *ACS Macro Lett.* **2018**, *7*, 699−704.

(27) Hore, M. J. A.; Ford, J.; Ohno, K.; Composto, R. J.; Hammouda, B. Direct Measurements of Polymer Brush Conformation Using Small-Angle Neutron Scattering (SANS) from Highly Grafted Iron Oxide Nanoparticles in Homopolymer Melts. *Macromolecules* **2013**, *46*, 9341−9348.

(28) Wei, Y.; Lang, X.; Hore, M. J. A. A correspondence between the Flory-Rehner theory for microgels and the Daoud-Cotton model for polymer-grafted nanoparticles. *J. Appl. Phys.* **2020**, *128*, No. 214701.

(29) Daoud, M.; Cotton, J. Star shaped polymers: a model for the conformation and its concentration dependence. *J. Phys.* **1982**, *43*, 531−538.

(30) Birshtein, T.; Zhulina, E. Conformations of star-branched macromolecules. *Polymer* **1984**, *25*, 1453−1461.

(31) Wijmans, C.; Zhulina, E. B. Polymer brushes at curved surfaces. *Macromolecules* **1993**, *26*, 7214−7224.

(32) Agrawal, A.; Wenning, B. M.; Choudhury, S.; Archer, L. A. Interactions, Structure, and Dynamics of Polymer-Tethered Nanoparticle Blends. *Langmuir* **2016**, *32*, 8698−8708.

(33) Agarwal, P.; Kim, S. A.; Archer, L. A. Crowded, Confined, and Frustrated: Dynamics of Molecules Tethered to Nanoparticles. *Phys. Rev. Lett.* **2012**, *109*, No. 258301.

(34) Poling-Skutvik, R.; Olafson, K. N.; Narayanan, S.; Stingaciu, L.; Faraone, A.; Conrad, J. C.; Krishnamoorti, R. Confined Dynamics of Grafted Polymer Chains in Solutions of Linear Polymer. *Macromolecules* **2017**, *50*, 7372−7379.

(35) Jiang, N.; Endoh, M. K.; Koga, T.; Masui, T.; Kishimoto, H.; Nagao, M.; Satija, S. K.; Taniguchi, T. Nanostructures and Dynamics of Macromolecules Bound to Attractive Filler Surfaces. *ACS Macro Lett.* **2015**, *4*, 838−842.

(36) de Gennes, P. Polymers at an interface; a simplified view. *Adv. Colloid Interface Sci.* **1987**, *27*, 189−209.

(37) Mark, C.; Holderer, O.; Allgaier, J.; Hübner, E.; Pyckhout-Hintzen, W.; Zamponi, M.; Radulescu, A.; Feoktystov, A.; Monkenbusch, M.; Jalarvo, N.; et al. Polymer chain conformation and dynamical confinement in a model one-component nano-composite. *Phys. Rev. Lett.* **2017**, *119*, No. 047801.

(38) Jiang, W.; Huang, J.; Wang, Y.; Laradji, M. Hydrodynamic interaction in polymer solutions simulated with dissipative particle dynamics. *J. Chem. Phys.* **2007**, *126*, No. 044901.

(39) Spenley, N. Scaling laws for polymers in dissipative particle dynamics. *Europhys. Lett.* **2000**, *49*, 534.

(40) Smith, G. D.; Bedrov, D.; Li, L.; Byutner, O. A molecular dynamics simulation study of the viscoelastic properties of polymer nanocomposites. *J. Chem. Phys.* **2002**, *117*, 9478−9489.

(41) Kalathi, J. T.; Kumar, S. K.; Rubinstein, M.; Grest, G. S. Rouse mode analysis of chain relaxation in polymer nanocomposites. *Soft Matter* **2015**, *11*, 4123−4132.

(42) Zhang, T.; Winey, K. I.; Riggleman, R. A. Polymer conformations and dynamics under confinement with two length scales. *Macro-molecules* **2019**, *52*, 217−226.

(43) Chremos, A.; Panagiotopoulos, A. Z.; Koch, D. L. Dynamics of solvent-free grafted nanoparticles. *J. Chem. Phys.* **2012**, *136*, No. 044902.

(44) Neha Biswas, P.; Kant, R. Theory for the Dynamics of Polymer Grafted Nanoparticle in Solution. *J. Phys. Chem. C* **2019**, *123*, 30657−30665.

(45) Groot, R. D.; Warren, P. B. Dissipative particle dynamics: Bridging the gap between atomistic and mesoscopic simulation. *J. Chem. Phys.* **1997**, *107*, 4423−4435.

(46) Kumar, S.; Larson, R. G. Brownian dynamics simulations of flexible polymers with spring-spring repulsions. *J. Chem. Phys.* **2001**, *114*, 6937−6941.

(47) Goujon, F.; Malfreyt, P.; Tildesley, D. J. Mesoscopic simulation of entanglements using dissipative particle dynamics: Application to polymer brushes. *J. Chem. Phys.* **2008**, *129*, No. 034902.

(48) Whittle, M.; Travis, K. P. Dynamic simulations of colloids by core-modified dissipative particle dynamics. *J. Chem. Phys.* **2010**, *132*, No. 124906.

(49) Doi, M.; Edwards, S. F. *The Theory of Polymer Dynamics*; Clarendon Press, 1988.

(50) Marciano, Y.; Brochard-Wyart, F. Normal modes of stretched polymer chains. *Macromolecules* **1995**, *28*, 985−990.

(51) Quake, S. R.; Babcock, H.; Chu, S. The dynamics of partially extended single molecules of DNA. *Nature* **1997**, *388*, 151−154.

(52) Wong, C. P. J.; Choi, P. Analysis of Brownian Dynamics and Molecular Dynamics Data of Unentangled Polymer Melts Using Proper Orthogonal Decomposition. *Macromol. Theory Simul.* **2019**, *28*, No. 1800072.

(53) Lang, X.; Lenart, W. R.; Sun, J. E.; Hammouda, B.; Hore, M. J. Interaction and conformation of aqueous poly (N-isopropylacrylamide)(PNIPAM) star polymers below the LCST. *Macromolecules* **2017**, *50*, 2145−2154.

(54) Richter, D.; Farago, B.; Fetters, L.; Huang, J.; Ewen, B. On the relation between structure and dynamics of star polymers in dilute solution. *Macromolecules* **1990**, *23*, 1845−1856.

(55) Zimm, B. H.; Kilb, R. W. Dynamics of branched polymer molecules in dilute solution. *J. Polym. Sci.* **1959**, *37*, 19−42.

(56) Arnold, A.; Bozorgui, B.; Frenkel, D.; Ha, B.-Y.; Jun, S. Unexpected relaxation dynamics of a self-avoiding polymer in cylindrical confinement. *J. Chem. Phys.* **2007**, *127*, No. 164903.

(57) Richter, D.; Kruteva, M. Polymer dynamics under confinement. *Soft Matter* **2019**, *15*, 7316−7349.

(58) Midya, J.; Rubinstein, M.; Kumar, S. K.; Nikoubashman, A. Structure of Polymer-Grafted Nanoparticle Melts. *ACS Nano* **2020**, *14*, 15505−15516.

(59) Jimenez, A. M.; Zhao, D.; Misquitta, K.; Jestin, J.; Kumar, S. K. Exchange Lifetimes of the Bound Polymer Layer on Silica Nano-particles. *ACS Macro Lett.* **2019**, *8*, 166−171.

(60) Lin, C.-C.; Gam, S.; Meth, J. S.; Clarke, N.; Winey, K. I.; Composto, R. J. Do. Attractive Polymer-Nanoparticle Interactions Retard Polymer Diffusion in Nanocomposites? *Macromolecules* **2013**, *46*, 4502−4509.